Measurement of AC Magnetic Field Distribution Using Magnetic Resonance Imaging

Y. Ziya Ider,* *Member, IEEE*, and L. Tugan Muftuler, *Member, IEEE*

Abstract—**Electric currents are applied to body in numerous applications in medicine such as electrical impedance tomography, cardiac defibrillation, electrocautery, and physiotherapy. If the magnetic field within a region is measured, the currents generating these fields can be calculated using the curl operator. In this study, magnetic fields generated within a phantom by currents passing through an external wire is measured using a magnetic resonance imaging (MRI) system. A pulse sequence that is originally designed for mapping static magnetic field inhomogeneity is adapted. AC current in the form of a burst sine wave is applied synchronously with the pulse sequence. The frequency of the applied current is in the audio range with an amplitude of 175-mA rms. It is shown that each voxel value of sequential images obtained by the proposed pulse sequence is modulated similar to a single-tone broadband frequency modulated (FM) waveform with the ac magnetic field strength determining the modulation index. An algorithm is developed to calculate the ac magnetic field intensity at each voxel using the frequency spectrum of the voxel signal. Experimental results show that the proposed algorithm can be used to calculate ac magnetic field distribution within a conducting sample that is placed in an MRI system.**

Index Terms— **Current density imaging, magnetic field measurement, magnetic resonance imaging.**

I. Introduction

MEASUREMENT of current density distribution inside a conducting object is desirable in several areas of investigation. Knowledge about the distribution of bioelectric currents inside the human body could be beneficial in solving the inverse problems of electrocardiography (ECG) and electroencephalography (EEG). Similarly, knowledge about the internal current distribution could be used to increase spatial resolution in electrical impedance tomography (EIT). In EIT, ac (1-kHz–500-kHz) currents are injected into a conducting object and surface voltage measurements are made. From these measurements, the internal conductivity distribution is reconstructed. In this imaging technique, resolution is low for regions distant from the surface because of the relative insensitivity of the surface voltage measurements to perturbations in conductivity values in these regions. On the other hand, if one could measure the inside current distribution, then one could possibly use this information to obtain high-resolution uniformly throughout the whole imaging region. In fact, it has been shown for 2-D objects that, in order to obtain such a uniform resolution it suffices to measure only the orthogonal component of the magnetic field generated by the internal current distribution [1], [2]. Another application, for which the internal current distribution could be sought, is when the spatial dependence of RF power deposition inside the body is to be optimized during therapeutic applications as well as in imaging techniques using application of RF fields (such as magnetic resonance tomography).

Scott *et al.* have used magnetic resonance imaging (MRI) techniques to measure the dc current density distribution inside an object [3]. The same investigators have extended their method to RF frequencies as well [4]. They can measure the distribution of RF currents injected to an object during a MRI data collection procedure. All these methods aim at measuring the magnetic fields generated by the current distribution, because the current density can be easily calculated using the curl operator if all three components, (x, y, z), of the magnetic field are known.

In this study, a new method is proposed to measure the ac magnetic field distribution in an object at audio frequencies. The study is confined to measuring the internal z-component of the ac magnetic field in a two-dimensional (2-D) object lying in the x-y plane. The method which is proposed in this study can be extended to measure the three-dimensional (3-D) magnetic field in a 3-D object as we have discussed in the discussion section. Since the aim of this study is to measure ac magnetic fields within a phantom, calculation of the current density distribution is not studied. Therefore, ac magnetic fields are generated by a current carrying wire external to the phantom to generate a known field distribution.

The proposed method makes use of a standard whole body MRI system. AC magnetic fields are induced in the 2-D conducting object while it is seated in the gantry of the MRI system. For this MRI system, a new pulse sequence and a new data collection procedure are designed and implemented. Also, an algorithm is proposed for processing the acquired data. Experimental results are reported and they show that the proposed methods are feasible and potentially useful.

II. Experimental Methods

A 0.15-T MRI system, developed in our laboratory [5], is used for data collection. The direction of the main dc

Manuscript received June 11, 1996; revised February 11, 1997. This work was supported by the Turkish Scientific and Technical Research Council (TUBITAK) under project EEEAG-128 and also by Middle East Technical University Research Fund under projectAFP-94-07-00-05. The Associate Editor responsible for coordinating the review of this paper and recommending its publication was X. Hu. *Asterisk indicates corresponding author.*

*Y. Z. Ider is with the Electrical and Electronics Engineering Department, Middle East Technical University, Ankara 06531 Turkey (e-mail: ideryz@rorqual.cc.metu.edu.tr).

L. T. Muftuler was is with the Electrical and Electronics Engineering Department, Middle East Technical University, Ankara 06531 Turkey. He is now with the Department of Radiological Sciences, University of California, Irvine CA 92697 USA.

Publisher Item Identifier S 0278-0062(97)07784-7.

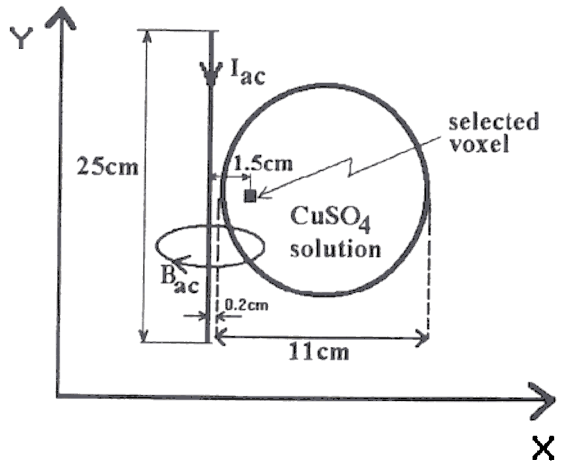

Fig. 1. Experimental setup which is used to acquire data. The ac magnetic field is measured within a cylindrical phantom filled with CuSO4 solution. The image voxel on which analysis is carried out is 1.5 cm away from the current carrying wire. The current carrying wire is 25-cm long and 5.7 cm away from the center of the disk. Wires leading to the 25-cm wire are not shown.

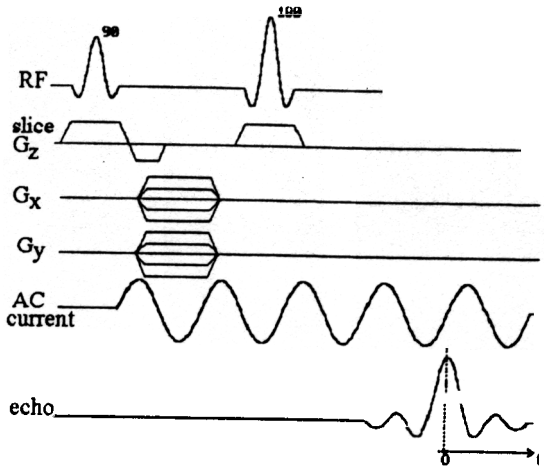

Fig. 2. MRI Pulse sequence and its relation to the applied current.

magnetic field of the MRI system is taken to be the z-direction. Experiments are carried out with the setup shown in Fig. 1. The object to be imaged is a disk with a thickness of 2.5 cm and a diameter of 11 cm, and it is placed such that its circular cross section is in the x-y plane. It is filled with a copper sulphate solution (1g/dl) to reduce the longitudinal and transverse spin relaxation times. A current carrying straight wire, 25-cm long, is placed 0.2 cm away from the side of the disk and directed along y-axis. The current in the wire generates magnetic fields within the object. Note that the generated fields are in the z-direction within the object. At this point it must be stressed that only fields which are parallel to the main magnetic field can be measured in MRI systems using our proposed method. The wires leading to and from the 25-cm wire are placed in the z-direction as long as possible. Therefore, distortion caused by these wires in the z-direction magnetic field in the plane of the disk is minimized.

Three experiments are performed. The first set of data is acquired with no ac current applied. The second set of data is acquired with a sine wave current at 200 Hz. In the third experiment a 100-Hz sine wave current is applied. For the last two experiments, the applied current is 175 ma (rms).

The MRI pulse sequence used in this study to acquire the data is given in Fig. 2. The first pulse applied is the 90° RF pulse (RF90). This pulse rotates the magnetic moment of the protons (termed as spins) from longitudinal direction to the transverse plane. Slice selection gradient pulse in z direction is applied together with the RF pulse to excite spins only within the selected slice. After the RF90, spatial encoding gradients in x and y directions are applied. The NMR signal is then recalled by a 180° RF refocusing pulse (RF180) and the resulting spin echo is recorded in the absence of any applied field gradient. The sine wave ac current is synchronized with the RF90 and it is started right after RF90 so that transients of the current applying circuit disappear before read out. This sine wave lasts for 120 ms (for this specific experiment, it could be as short as 49.4 ms). Data collection starts at 21 ms after the beginning of ac current and lasts for 28.4 ms. From the echo signal, 128 samples are recorded. This complete cycle shown in Fig. 2 is repeated every 400 ms (repetition time). Each time this sequence is repeated, the values of G_x and G_y are changed such that $G_x = g_x * m$ and $G_y = g_y * n$ for all values of $m = -16$ to 15 and $n = -16$ to 15 where g_x and g_y are constant and define the step size in spatial frequency domain. The time interval between the peak of RF90 and the peak of the echo signal (Echo Time) is 36.5 ms and the sampling rate is 4500 Hz. The whole data collection is repeated two times and the two sets of data are averaged in order to improve SNR. Imaging region is 20 cm*20 cm.

Raw data sets are processed by software which are developed using BORLANDC 3.1 and MATLAB.

III. Theory

In the absence of an internal ac magnetic field distribution, the pulse sequence shown in Fig. 2 is the same as the one used by Maudsley *et al.* to calculate the z-component of the main magnetic field inhomogeneity [6]. During the observation period, if there is no internal ac magnetic field distribution, the spins evolve under the influence of the z-component of the static magnetic field inhomogeneity, $B(x,y)\cdot\boldsymbol{k}$, only, where $\boldsymbol{k}$ is the unit vector in z-direction. If also a time varying (ac) magnetic field $b(x,y)\cos(wt+\alpha)\cdot\boldsymbol{k}$ is added to the static magnetic field inhomogeneity, where α is arbitrary but fixed, then the equation of the spin echo signal becomes [7]

$$s(u,v,t) = \iint M(x,y)e^{j\theta}e^{j(xu+yv)} \cdot e^{j\gamma\int_0^t (B(x,y)+b(x,y)\cos(wt))\,dt}\,dx\,dy$$

or

$$s(u,v,t) = \iint M(x,y)e^{j\theta}e^{j(xu+yv)} \cdot e^{j\gamma(B(x,y)t+b(x,y)\sin(wt)/w)}\,dx\,dy. \quad (1$$

$M(x,y)$ is a measure of the density of protons within a voxel at coordinates (x,y). The phase angle accounts for all the constant phase terms accumulated. This phase term does not affect our calculations, therefore, it will be included in the magnetization vector, $M(x,y)$, and will not be considered

further. γ is a constant called "gyromagnetic ratio" and its value is 4.26*107 Hz/Tesla for protons (Hydrogen atom). u and v in this equation are termed as "spatial frequencies" and are defined as $u = \gamma \cdot G_x \cdot T_G$ and $v = \gamma \cdot G_y \cdot T_G$, where T_G is a constant, representing the duration of the gradient pulses.

By sampling $s(u,v,t)$ in (u,v,t) axes, one obtains a 3-D data matrix from which 2-D matrices are extracted. Each 2-D matrix contains elements of $s(u,v,t)$ at a fixed time t for changing values of G_x and G_y (or, equivalently, of u and v). Two–dimensional Fourier transform ($\mathrm{FT}_2\{\cdot\}$) with respect to u and v is applied to each 2-D matrix. This operation transforms the data from spatial frequency domain to the space domain. Thus, if

$$S(x,y,t) = \mathrm{FT}_2\{s(u,v,t)\}, \quad \text{then}$$
$$S(x,y,t) = M(x,y)e^{j\gamma(B(x,y)t + b(x,y)\sin(wt)/w)} \tag{2}$$

By defining $m_f(x,y) = \gamma \cdot b(x,y)/w$ and $w_c(x,y) = \gamma B(x,y)$, (2) becomes

$$S(x,y,t) = M(x,y)e^{jw_c(x,y)t}e^{jm_f(x,y)\sin(wt)}. \tag{3}$$

For any voxel located at (x,y), $S(x,y,t)$ will be referred to as the voxel signal. From (3), it is seen that the voxel signal has the form of a single-tone wide band frequency modulated (FM) signal [8].

The Fourier series representation of (3) is given as

$$S(x,y,t) = M(x,y)\sum_{n=-\infty}^{\infty} J_n(m_f(x,y))e^{j(w_c(x,y)+nw)t}. \tag{4}$$

$J_n(m_f(x,y))$ is the Bessel function of the first kind of order n and argument m_f. A plot of these functions up to fourth order is given in Fig. 3. In communication theory, $m_f(x,y)$ is called the "modulation index," w_c is called the "carrier frequency" and w is the "modulation frequency." We arrive at several conclusions from (4).

1) If no ac magnetic field exists, $m_f(x,y) = 0$, and, therefore, $J_0(m_f(x,y)) = 1$ and all higher-order Bessel functions are zero. This results in a single peak at frequency w_c in the frequency spectrum of the voxel signal.
2) If an ac magnetic field is applied, the spectrum of the voxel signal contains a carrier component at frequency w_c and an infinite set of side frequencies located symmetrically on either side of the carrier at frequency offsets of $w, 2w, 3w, \cdots$.
3) For small values of m_f, the magnitude of J_0 is large and magnitudes of higher-order Bessel Functions are close to zero. Thus, the detectability of the side lobes decreases if the amplitude of the applied current is decreased or its frequency is increased.

Using (4) and the frequency spectrum of voxel signal for each space coordinate, it is possible to calculate the ac magnetic field intensity, $b(x,y)$, within the object to be imaged. Let P_0 and P_1 be the measured magnitudes of the central peak and the first side peak of the frequency spectrum of the voxel signal, respectively. Magnitudes of these peaks are obtained from the magnitude of the spectrum. The polarity of their ratio is obtained by observing the difference of the phases of the peaks in the spectrum. From (4) it is clear that, the ratio $R = P_0/P_1$ must be equal to $J_0(m_f(x,y))/J_1(m_f(x,y))$.

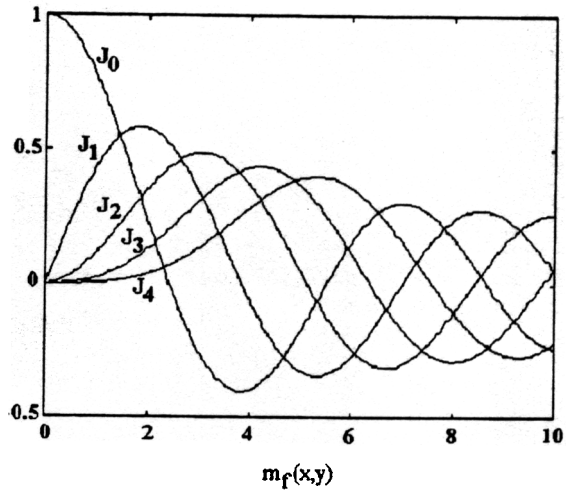

Fig. 3. Bessel functions of the first kind as a function of m_f. Only the functions up to fourth order are drawn.

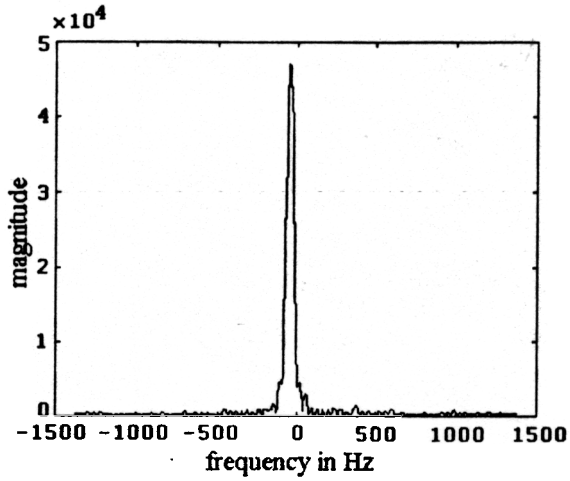

Fig. 4. Magnitude of the frequency spectrum of the voxel signal for the case of no ac current applied (arbitrary units). Observations are for the voxel shown in Fig. 1.

For a measured value of R we found $m_f(x,y)$ by finding the root of the equation

$$R - J_0(m_f(x,y))/J_1(m_f(x,y)) = 0 \tag{5}$$

by using the Bessel functions and nonlinear function minimizing routine *FSOLVE* of MATLAB. This routine uses Gauss–Newton method with a mixed quadratic and cubic line search method. Precision of the required solution was selected to be 10^{-4}. The initial value for m_f was given as 0.01 and the solution invariably converges to a value between 0 and 3.8 (at approximately 3.8, J_1 has its first zero crossing). It is explained in the discussion that within this range (5) has a unique solution.

At this point it must be stated that the 128-point voxel signals are padded with zeros to obtain a 1024-point sequence before fast Fourier transform (FFT) is applied, to increase frequency resolution in the FFT calculations. The sampling

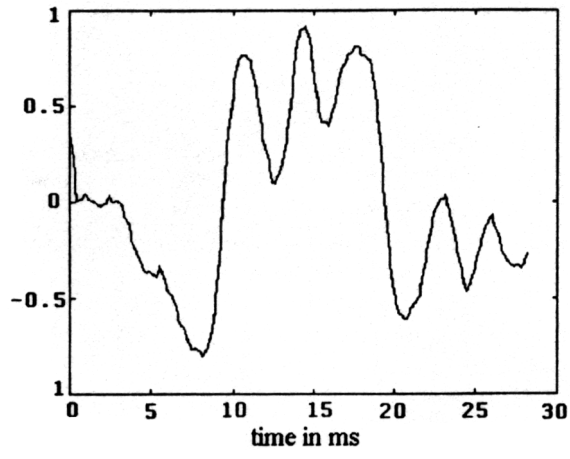

(a)

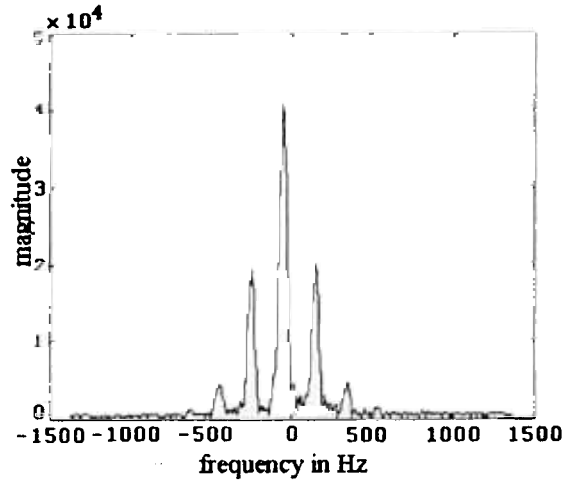

(b)

Fig. 5. (a) Real part of the voxel signal for the case of 200-Hz ac current application (normalized units). (b) Magnitude of the frequency spectrum of the voxel signal (arbitrary units). Observations are for the voxel shown in Fig. 1.

window that we use is 28.4 ms. This means the side lobes that we see in the spectrum (which are ideally impulse functions) will spread by $2 \cdot 1/28.4$ ms which is equal to ± 35 Hz. Even with the 100 Hz ac field application case the ± 35 spread will not be a problem.

IV. Results

Time variation of the value of the voxel indicated in Fig. 1 is investigated under different experimental conditions. For the case of no applied ac current, the magnitude of the Fourier transform of the voxel signal is drawn in Fig. 4. In the Fourier transform there is only a single peak. The frequency of this peak is proportional to the static field inhomogeneity at that voxel [defined as w_c in (3)].

Results for the case of 200-Hz ac current application are shown in Fig. 5. Side frequency peaks with 200 Hz separation can be clearly seen in this figure. The case of 100 Hz modulation is illustrated in Fig. 6. In this figure, the side frequency peaks are separated by 100 Hz as expected. It is also observed that, the amplitude of the side frequency peaks relative to the central peak are significantly larger for the case of 100-Hz modulation as compared to the case of

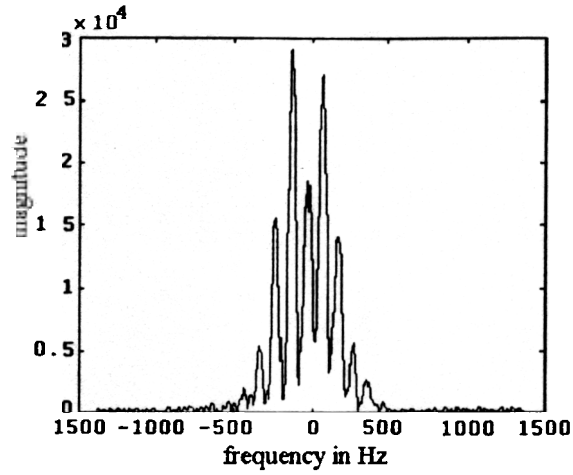

Fig. 6. Magnitude of the frequency spectrum of the voxel signal when 100-Hz ac current is applied (arbitrary units). Observations are for the voxel shown in Fig. 1.

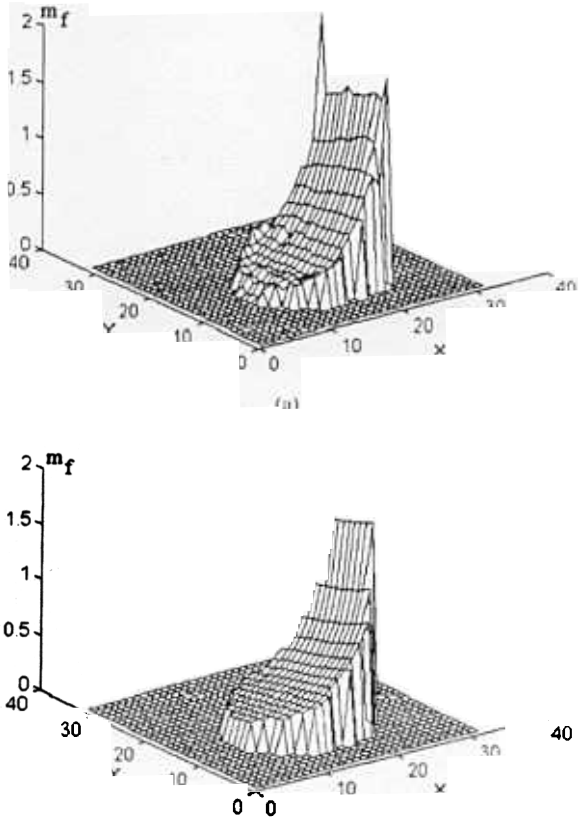

(b)

Fig. 7. (a) Measured modulation index (m_f) distribution within the phantom shown in Fig. 1, calculated from the data acquired when 100-Hz, 175-mA current is applied. (b) m_f distribution calculated at the center of each voxel using Biot–Savart law for the same geometry and experimental conditions.

200-Hz modulation. The argument of the Bessel functions, $m_f(x, y)$ in (4), is inversely proportional to frequency, as shown in (3) and, therefore, it is indeed expected that side lobe amplitudes increase as the frequency decreases, provided that the argument is less than 3.8. Indeed, using the ratio of the first side peak magnitude to the central peak magnitude, and the method explained in Section III, the value of m_f is calculated to be 1.7 and 0.89 for the 100-Hz and 200-Hz cases, respectively.

Using the relations given in (3) and the calculated values of m_f, the value of ac field at the considered voxel is calculated to be 0.0399 Gauss and 0.0417 Gauss for the 100-Hz and 200-Hz cases respectively. Since the applied current magnitude is the same in both cases, the magnitude of the ac magnetic field must also be the same. The difference in the calculated values reflect the effect of noise and experimental errors. The value of the field was also calculated by the Biot–Savart law for the actual current wire geometry and this value was found to be 0.033 Gauss.

In order to find out if any systematic errors are made or not, the measured 2-D distribution of the modulation index $m_f(x,y)$ is also displayed in Fig. 7(a). This distribution is calculated from the data acquired when 100-Hz, 175-mA current is applied. The magnetic field distribution, $b(x,y)$, is calculated also by Biot–Savart law for the same geometry and experimental conditions. From this expected field distribution, the $m_f(x,y)$ distribution is calculated and it is illustrated in Fig. 7(b). The measured and the calculated distributions exhibit approximately $(1/r)$ type dependence, which is the expected spatial dependence of the magnetic field generated by a straight current carrying wire.

V. Conclusion and Discussion

We have shown by derivation that the presence of an ac magnetic field in z-direction results in an FM type time dependence of the voxel values of the sequential images obtained by the pulse sequence used in this study. We have also shown that the experimental results are very much in line with this theory. It must also be noted that the present method, which models the voxel signal as an FM signal, has proved to be very useful in determining the sampling rate and the length of the data acquisition window.

The magnetic field distribution that we have calculated by Biot–Savart Law and as shown in Fig. 7(b) is just an approximation. We have ignored the magnetic fields generated by currents in the wires which connect the straight wire to the current source. Moreover, the voxel size in the experiment is roughly 7 mm · 7 mm · 20 mm. Therefore, the field measured by our method may not match with the value calculated at the center of the pixel using Biot–Savart law, especially in view of the $1/r$ dependence of the magnetic field generated by a single line. On the other hand, the field value calculated by Biot–Savart Law at the center of the voxel shown in Fig. 1 (0.033 Gauss) is 6% different than the field calculated at 1 mm away from the center toward the wire (0.035 Gauss). Therefore, the large pixel size can be a major source of error between the calculated and measured values. There are also measurement errors, namely, errors in finding the peaks of the spectrum lobes and random noise in the signals. Despite these possible sources of errors, the difference between the calculated and measured magnetic fields does not exceed 20%.

From (3) it is seen that $m_f(x,y)$ decreases with decreasing amplitude or increasing frequency of the applied current. This causes the magnitude of the side peaks in the frequency spectrum of the voxel signal to become comparable to noise and, therefore, errors in the calculation of $b(x,y)$ increase. In order to increase the side lobe amplitudes, one may choose to use a higher field MRI system. A higher dc magnetic field will increase the magnitude of the magnetization vector $M(x,y)$ and, therefore, all side lobes will increase in amplitude as seen in (4). However the noise in the spectrum will not increase in the same proportion because, it is well known that in higher field MRI systems SNR is higher [9]. For example, if a 0.47-T MRI system is used, a fivefold increase in SNR may be expected compared to that of a 0.15-T system [9]. Hence, with a high field MRI system, it may be possible to measure magnetic fields generated by currents with lower amplitude and higher frequency. It is also possible to increase SNR by increasing the number of averaged data sets. However, the imaging sequence lasts 13 min and 40 s with two data sets averaged. Therefore, long imaging times must be considered as the number of sampling averages are increased.

Static magnetic field inhomogeneity is approximately within ±30 ppm in the imaging region, which corresponds to ±192-Hz shift in frequency. Chemical shift is not significant at 0.15-T field strength. Since our signal is an FM signal, its bandwidth is much larger than the frequency of the modulating signal plus center frequency due to dc field offset (sidelobes at harmonics of modulating frequency appear). Our analog filter before digitization has a cutoff at 2250 Hz and our sampling frequency is 4500 Hz. Therefore, for a modulation frequency of 200 Hz, up to ten sidelobes fall within the bandwidth of our signal acquisition system. Since we only use J_0/J_1 ratio, a much smaller bandwidth would suffice, however, in order to verify our theory and not to exclude the possibility of using higher sidelobes in our calculations, we decided to use a 2250-Hz lowpass filter.

In our experiments, the applied current and, therefore, the magnetic field generated by this current were large compared to what one may encounter in a real medical EIT experiment. Therefore, in future studies, the lower limit of the applied currents will have to be established in order to understand if these new methods are appropriate, for example for medical EIT. So far we can claim that in nonmedical EIT applications the magnetic fields generated by the currents flowing in the imaged object can be measured using MRI. Once the magnetic field distribution is measured (at least in three directions), one can calculate the currents generating these magnetic fields. In theory, any information about the internal current distribution can be incorporated into the EIT reconstruction algorithms in order to increase spatial resolution, especially for interior regions of the imaged object. However, it may not be necessary to calculate the currents and it may suffice to incorporate the magnetic field information directly into the reconstruction algorithm. Simulation studies [1], [2] have shown that knowledge of the magnetic field distribution within the object in an EIT experiment improves the resolution of the obtained conductivity distribution image in regions distant from the surface. The frequency of the applied current was also lower than those used in medical EIT experiments. The reason for selecting a lower frequency value was to utilize a large m_f value and, thus, to reduce errors in the measurement of the ac magnetic field.

In Section II, it was mentioned that the ac fields which are in the same direction with the main dc magnetic field of the

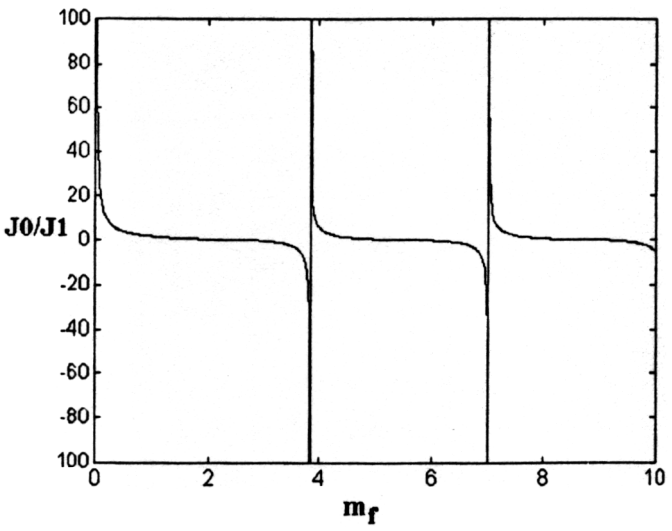

Fig. 8. Ratio of zeroth- and first-order Bessel Functions, J_0/J_1, as a function of m_f. Note that the function is one-to-one within the interval (0, 3.8).

MRI magnet (z-direction) can be measured with the proposed method. We might note as well that the z-component of the magnetic field in a 3-D object can be measured by using multislice imaging methods without increasing the imaging time. Within the TR interval of 400 ms, used in our study, one can simultaneously image seven slices. To calculate current density, one has to measure magnetic fields in the other directions (x, y) also. These fields can be calculated from separate data sets acquired from successive experiments. In each experiment, the object is to be rotated within the MRI magnet so that the x- or y-axis of the object coincides with the z-axis of the magnet. After the field is calculated in all three directions, the current density can be computed by taking the curl of this field.

The experiments described in this paper are designed to generate ac magnetic fields within a phantom by passing current through an external wire. The advantage of using an external wire is the use of Biot–Savart law to calculate the magnetic field in the phantom. In an EIT experiment, current is injected into a phantom and a numerically more involved method such as the finite element method is required to calculate the magnetic field generated by these injected currents.

It must also be emphasized that the eddy currents generated within the phantom will not be significant, since the frequency of the applied currents is low and the resistivity of the solution is high (no salt is added). Therefore, the secondary magnetic fields generated by the eddy currents will not be significant also.

The ratio of Bessel functions, J_0/J_1 is a monotonically decreasing function within the interval of modulation index (m_f) values from 0 to 3.8. For a domain of $0 < m_f < 3.8$, the range of J_0/J_1 ratio is from $-\infty$ to $+\infty$. However, this same range of J_0/J_1 ratio is generated by other domains of m_f as seen in Fig. 8. Therefore, provided that m_f is between 0 and 3.8, one can find a unique solution to (5). However, a higher-order Bessel function has its first zero crossing at a larger m_f value. This yields a monotonically decreasing J_0/J_2 ratio, for example, for a wider range of m_f values. Therefore, by including the information contained in the peaks of higher-order Bessel functions, we can measure the field values within a wide range. In this study, with the current amplitude and frequency ranges that we used, the m_f values stayed in the interval (0, 3.8) as can be seen in Fig. 7(a). Therefore, in this study we did not use the information contained in the higher-order Bessel functions. It is also evident from Fig. 7(a) and 7(b) that a systematic error was not made in calculating m_f. However, it is still necessary to develop an algorithm which has a wider range of unique solution possibility.

The results of the experiments reported in this paper validate our formulations and give a measure of our accuracy. In future studies, the field distribution generated by injecting currents into a phantom will be measured and the effects of internal conductivity pattern on this distribution will be investigated.

REFERENCES

[1] O. Birgul and Y. Z. Ider, "Use of the magnetic field generated by the internal distribution of injected currents for electrical impedance tomography," in *Proc. 9th Int. Conf. Electrical Bioimpedance in conjunction with European Community Concerted Action on Impedance Tomography*, Sept. 26–30, 1995, pp. 418–419.

[2] ——, "Electrical impedance tomography using the magnetic field generated by injected currents," presented at 18th Int. Annu. Mtg. IEEE EMBS, Oct. 31–Nov. 3, 1996, Amsterdam, The Netherlands.

[3] G. C. Scott, M. L. G. Roy, R. L. Armstrong, and R. M. Henkelman, "Measurement of nonuniform current density by magnetic resonance," *IEEE Trans. Med. Imag.*, vol. 10, pp. 362–374, 1991.

[4] G. C. Scott, M. L. G. Joy, R. L. Armstrong, and R. M. Henkelman, "Electromagnetic considerations for RF current density imaging," *IEEE Trans. Med. Imag.*, vol. 14, pp. 515–524, 1995.

[5] L. T. Muftuler, Y. Z. Ider, H. Koymen, C. Tarakci, and E. Turan, "Low cost PC based whole body magnetic resonance imaging system," in *Proc. 15th Int. Annu. Mtg. IEEE EMBS*, San Diego, CA, Oct. 28–31, 1993, pp. 184–185.

[6] A. A. Maudsley, H. E. Simon, and S. K. Hilal, "Magnetic field measurement by NMR imaging" *J. Phys. E: Sci. Instrum.*, vol. 17, pp. 216–220, 1984.

[7] Y. Z. Ider, L. T. Muftuler, and O. Birgul, "Use of MRI for measuring ac internal currents of EIT: A feasibility study," in *Proc. 9th Int. Conf. Electrical Bioimpedance in conjunction with European Community Concerted Action on Impedance Tomography*, Sept. 26–30, 1995, pp. 420–421.

[8] S. Haykin, *Communication Systems*. New York: Wiley, 1983, pp. 180–219.

[9] L. E. Crooks, M. Arakawa, J. Hoenninger, B. McCarten, J. Watts, and L. Kaufman, "Magnetic resonance imaging: Effects of magnetic field strength," *Radiol.*, vol. 151, pp. 127–133, 1984.